Evidence for the role of instantons in hadron structure from lattice QCD

M.-C. Chu
W. K. Kellogg Radiation Laboratory, Caltech 106-38, Pasadena, California 91125

J. M. Grandy
T-8 Group, MS B-285, Los Alamos National Laboratory, Los Alamos, New Mexico 87545

S. Huang
Department of Physics, FM-15, University of Washington, Seattle, Washington 98195
and Center for Theoretical Physics, Laboratory for Nuclear Science and Department of Physics, Massachusetts Institute of Technology, Cambridge, Massachusetts 02139

J. W. Negele
Center for Theoretical Physics, Laboratory for Nuclear Science and Department of Physics, Massachusetts Institute of Technology, Cambridge, Massachusetts 02139
(Received 29 December 1993)

Cooling is used as a filter on a set of gluon fields sampling the Wilson action to selectively remove essentially all fluctuations of the gluon field except for the instantons. The close agreement between quenched lattice QCD results with cooled and uncooled configurations for vacuum correlation functions of hadronic currents and for density-density correlation functions in hadronic bound states provides strong evidence for the dominant role of instantons in determining light hadron structure and quark propagation in the QCD vacuum.

PACS number(s): 12.38.Gc

I. INTRODUCTION

Understanding the quark and gluon substructure of hadrons is particularly challenging because none of the standard analytic techniques of theoretical physics is applicable to the nonperturbative solution of QCD. Indeed, these standard techniques do not even provide a qualitative understanding of the mechanism responsible for the gross structure of hadrons—whether it is the Coulomb-like interaction between quarks arising from short wavelength fluctuations of the gluon field, the behavior at large distances associated with confinement, or a mechanism associated with topological structures in the QCD vacuum corresponding in the semiclassical limit to instantons.

The goal of this work is to use lattice QCD as a tool to understand the role of instantons in determining the gross features of the structure of hadrons and of the propagation of quarks in the QCD vacuum. Thus in this work we use lattice QCD as a means to obtain physics insight into issues which are not experimentally accessible rather than to calculate experimental observables.

Our strategy for elucidating the role of instantons in hadron structure is to focus on correlation functions which characterize the gross structure of hadrons and quark propagation in the QCD vacuum and which are well described by quenched lattice QCD calculations which sample the full Wilson action. These calculations include all the fluctuations and topological excitations of the gluon field and thus include the full perturbative and nonperturbative effects of the short range Coulomb and hyperfine interactions, confinement, and instantons. We then use cooling as described below to remove essentially all fluctuations of the gluon field except for the instantons which, because of their topology, cannot be removed by local minimization of the action. Thus, both the Coulomb interaction and confinement are almost completely removed while retaining most of the instanton content. To the extent to which the gross features of hadron structure and quark propagation in the QCD vacuum are unaffected by removing all the gluonic modes except instantons, we have strong evidence for the dominant role of instantons.

The vacuum correlation functions we consider are the point-to-point equal-time correlation functions of hadronic currents $R(x) = \langle \Omega | T J(x) \bar{J}(0) | \Omega \rangle$ discussed in detail in an extensive review by Shuryak [1] and recently calculated in quenched lattice QCD [2]. These correlation functions characterize the propagation of quarks and antiquarks in all the relevant hadronic channels and complement bound state data in the same way as nucleon-nucleon scattering phase shifts complement deuteron properties in characterizing the nuclear interaction. Two results of Refs. [1] and [2] are of particular relevance to the present work. First, the quenched lattice calculations of the correlation functions agree well with the dispersion relation analysis of experimental data in all channels for which data are available (pseudoscalar, vector, and axial vector) indicating that quenched QCD with present lattice technology describes the gross features of quark propagation in the vacuum. Second, the random instanton model also agrees reasonably well with

the empirical results in these channels and with the lattice results in all other channels, indicating that if the instanton content of the QCD vacuum were similar to that parametrized in this model, the instantons also could account for the essential features of quark propagation.

To characterize the gross properties of hadrons, in addition to the mass, we consider quark density-density correlation functions [3–5] $\langle h|\rho(x)\,\rho(0)|h\rangle$. In contrast with wave functions, which have large contributions from the gluon wave functional associated with the gauge choice or definition of a gauge-invariant amplitude [6], the density-density correlation function is a gauge-invariant physical observable which directly specifies the spatial distribution of quarks. Comparison of these correlation functions in full quenched QCD and retaining only the instanton content of the gluon configuration is therefore expected to provide a quantitative indication of the role of instantons in determining the spatial distribution of quarks in hadrons.

This present work is strongly motivated by the physical arguments and instanton models of QCD by Shuryak and collaborators [7,8] and by Dyakanov and Petrov [9]. The basic picture is that although the dilute instanton gas approximation is inconsistent because the instanton probability increases with its size, when the interactions of instantons are taken into account, the vacuum may be characterized by a dense, stable distribution of instantons. The zero modes of massless quarks associated with these instantons correspond to localized quark states, and the propagation of light quarks takes place primarily by hopping between these localized states. In the simplest version of the model [8], the instanton vacuum is characterized by a random spatial and color distribution of instantons and anti-instantons of a single radial size ρ and density n. For subsequent reference, we note that when ρ is chosen to be $\frac{1}{3}$ fm to fit the vacuum gluon condensate and n is chosen to be 1 fm^{-4} to fit the vacuum quark condensate, the random instanton vacuum model results in Ref. [8] yield a good description of the vacuum correlation functions.

The outline of the paper is as follows. In Sec. II, we describe the lattice calculation. The results for the instanton content of the vacuum are presented in Sec. III, where we characterize the size and density of instantons in cooled configurations and indicate the degree to which other gluon fluctuations are removed. Hadronic observables in the cooled vacuum are presented and discussed in Sec. IV and the summary and conclusions are given in the final section.

II. LATTICE CALCULATIONS

As discussed in the Introduction, we use cooling [10,11] as a filter to extract the instanton content of 19 gluon configurations obtained by sampling the standard Wilson action on a $16^3\times 24$ lattice at $\frac{6}{g^2}=5.7$. A configuration is cooled by an iterated sequence of relaxation steps, where for each step, the action is minimized locally at every link of the lattice using the Cabibbo-Marinari [12] algorithm with three SU(2) subgroups and $\beta=\infty$. Although it is difficult to characterize the results of cooling precisely, it is clear that short wavelength, local fluctuations are removed most rapidly by cooling steps, and topologically stabilized instanton excitations are removed most slowly. [Although isolated instantons can slowly shrink and eventually disappear with extended cooling because of $O(a^2)$ errors in the lattice action, the primary mode of removal is instanton–anti-instanton annihilation.] Thus, as the number of cooling steps increases, the instanton content of the configuration is strongly enhanced relative to all other gluon excitations.

To express this effect of cooling precisely, it is useful to write the expectation value of an operator O in uncooled and cooled configurations as

$$\langle O\rangle = \frac{\int \mathcal{D}[U]\,O[U]\,e^{-S[U]}}{\int \mathcal{D}[U]\,e^{-S[U]}} \tag{2.1a}$$

and

$$\langle O\rangle_n = \frac{\int \mathcal{D}[U]\,O\,[f_n[U]]\;e^{-S[U]}}{\int \mathcal{D}[U]\,e^{-S[U]}}\;, \tag{2.1b}$$

where $f_n[U]$ denotes the configuration of SU(3) elements obtained deterministically by applying n cooling steps to the configuration U. Then, by inserting $1=\int \mathcal{D}[V]\delta[V-f_n[U]]$, we may write

$$\langle O\rangle_n = \frac{\int \mathcal{D}[V]\,O[V]\,e^{-\tilde{S}_n[V]}}{\int \mathcal{D}[V]\,e^{-\tilde{S}_n[V]}}\;, \tag{2.1c}$$

where $e^{-\tilde{S}_n[V]}\equiv\int \mathcal{D}[U]\,\delta\,[V-f_n[U]]\;e^{-S[U]}$ is an effective action defining the distribution of cooled configurations. Hence, the expectation value in the cooled configuration may be expressed

$$\langle O\rangle_n = \frac{\int \mathcal{D}[U]\,O[U]\,e^{-\left(\tilde{S}_n[U]-S[U]\right)}\,e^{-S[U]}}{\int \mathcal{D}[U]\,e^{-S[U]}}\;, \tag{2.1d}$$

so that the filtering factor is seen to be $e^{-\left(\tilde{S}_n[U]-S[U]\right)}$. For large scale, topologically stabilized modes present equally in $\tilde{S}$ and S, this filtering factor approaches 1, while for short wavelength fluctuations effectively removed by cooling, it approaches 0.

To monitor the filtering of different degrees of freedom as a function of cooling steps, we measure several relevant gluonic observables. Short wavelength fluctuations giving rise to the perturbative Coulomb and hyperfine interactions are reflected in the total action S, and when S is reduced by several orders of magnitude, it is clear that these modes have been strongly filtered. Denoting the action associated with a single instanton $S_0=\frac{8\pi^2}{g^2}$, once $\frac{S}{S_0}$ equals the number of instantons plus anti-instantons, we know all other excitations have essentially been removed.

Similarly, we monitor confinement by measuring the string tension extracted from a 4×7 Wilson loop. The size of the Wilson loop is relevant, since the local minimization of the action corresponds to replacing each link by the sum of staples made up of the other three links of each plaquette to which the original link contributes.

Thus, each cooling step replaces a Wilson loop by a bundle of loops smeared by at most one lattice site. So, as long as the number of cooling steps is much smaller than the size of the loop, one must still see confinement. However, once the number of steps is larger than the loop size, there is nothing to prohibit the string tension from going to zero. The 4×7 Wilson loops were chosen as a measure of confinement for the practical reason that these were the largest loops that were already available from an earlier calculation at the same value of β with the same cooling algorithm [13].

Finally, to monitor the instanton content, we measure the topological charge $\langle Q \rangle$ and topological susceptibility $\langle Q^2 \rangle$, where

$$Q = \sum_{x_n} Q(x_n) \ , \tag{2.2}$$

and we use the simplest expression for the topological charge density,

$$Q(x_n) = -\frac{1}{32\pi^2} \epsilon_{\mu\nu\rho\sigma} \ \mathrm{Re\,Tr}\ [U_{\mu\nu}(x_n)\, U_{\rho\sigma}(x_n)] \ . \tag{2.3}$$

Although this expression for the topological charge density is known to be inadequate for the large fluctuations occurring in uncooled configurations, it is adequate for the smooth configurations which emerge after several cooling steps. For subsequent reference, one should note that for a random ensemble of Poisson-distributed instantons and anti-instantons, $\langle Q \rangle = 0$ and $\langle Q^2 \rangle = I + A$, the number of instantons plus anti-instantons.

As explained in the Introduction, we characterize the propagation of quarks in the vacuum by the vacuum correlation functions $R(x) = \langle \Omega | T\, J(x)\, \bar{J}(0) | \Omega \rangle$. Specifically, as in Ref. [2], we calculate the following correlation functions in the indicated channels:

pseudoscalar,

$$R(x) = \langle \Omega | T J^p(x) \bar{J}^p(0) | \Omega \rangle ;$$

vector,

$$R(x) = \langle \Omega | T J_\mu(x) \bar{J}_\mu(0) | \Omega \rangle ;$$

nucleon,

$$R(x) = \tfrac{1}{4} \mathrm{Tr} [\langle \Omega | T J^N(x) \bar{J}^N(0) | \Omega \rangle x_\nu \gamma_\nu] ;$$

Δ,

$$R(x) = \tfrac{1}{4} \mathrm{Tr} (\langle \Omega | T J^\Delta_\mu(x) \bar{J}^\Delta_\mu(0) | \Omega \rangle x_\nu \gamma_\nu) ;$$

$$J^p = \bar{u}\, \gamma_5\, d \ , \tag{2.4a}$$

$$J_\mu = \bar{u}\, \gamma_\mu\, \gamma_5\, d \ , \tag{2.4b}$$

$$J^N = \epsilon_{abc} [u^a\, C\, \gamma_\mu\, u^b]\, \gamma_\mu\, \gamma_5\, d^c \ , \tag{2.4c}$$

$$J^\Delta_\mu = \epsilon_{abc} [u^a\, C\, \gamma_\mu\, u^b]\, u^c \ . \tag{2.4d}$$

As in Refs. [1] and [2], we consider the ratio of the correlation function in QCD to the correlation function for noninteracting massless quarks, $\frac{R(x)}{R_0(x)}$, which approaches 1 as $x \to 0$ and displays a broad range of nonperturbative effects for x of the order of 1 fm. As described in Ref. [2], the effects of lattice anisotropy are removed by calculating $R_0(x)$ on the same lattice as $R(x)$ and measuring the ratio for a cone of lattice sites concentrated around the diagonal. Finite lattice volume effects are corrected by subtracting the contributions of first images as in Ref. [2]. Finally, the correlation functions are fit as in Ref. [2] by a spectral function parametrized by a resonance mass, the coupling to the resonance, and the continuum threshold.

Hadron density correlation functions are calculated as in Refs. [4] and [5] for the pion, ρ, and nucleon. To avoid calculating propagators between density operators, we consider the correlation functions

$$\langle h | \rho_u(x) \rho_d(0) | h \rangle \propto \int d^4y\, \langle T\, J_h(0,T)\, \bar{u}\, \gamma_0\, u(x+y,t)\, \bar{d}\, \gamma_0\, d(y,t)\, J_h(0,0) \rangle \ , \tag{2.5}$$

where J_h denotes a point π, ρ, or N source and the correlation function is averaged over the central two time slices. Image corrections for finite volume effects are applied as in Ref. [14].

A significant conceptual issue in comparing observables calculated using cooled configurations with uncooled results is how to change the renormalization of the bare mass and coupling constant as the gluon configurations are cooled. Clearly, as the fluctuations corresponding to gluon exchange are filtered out, the gluonic contribution to the physical mass and coupling constant change significantly, and so our task is to find the most physical scheme to determine the hopping parameter κ and the lattice spacing a. A different, but equivalent way to state the issue is to note that the cooled calculation samples a different action, Eq. (2.1c). For the full theory, of course, the result should not depend on the choice of the masses or other observables used to determine κ and a. However, after filtering out all the gluonic excitations except instantons, there is no reason that all physical observables should be correctly reproduced, and so different values of κ and a (as well as all other observables) will arise from different choices of a pair of observables to determine the parameters of the theory. Since we are primarily interested in the instantons after cooling, the most natural quantity to use to determine a would be the topological susceptibility χ. However, given the limitations of the naive topological charge density [15], the uncooled lattice measurement of χ is unreliable, and so there would be a large uncertainty in using it to determine a. (We will see below that if we did use this prescription, a would be essentially independent of cooling.)

In the end, we have chosen to use the physical pion and nucleon masses to determine κ and a for the cooled

configurations. As expected, the critical kappa κ_c approaches the free field value 0.125 with increasing cooling. To the accuracy of our present calculations there is not a significant difference between extrapolating to κ_c and to the physical pion mass, and so results are quite insensitive to this choice. As will be seen below, a changes by $\sim 16\%$ after 25 cooling steps when the nucleon mass is used to set the scale, and within errors, the ρ mass remains unchanged after cooling with this value of a. The other extreme would be to keep a fixed at the uncooled value and thus display what remains in the original path integral when only instantons are retained. This constant a would also be consistent with the constant topological susceptibility. It is a remarkable result that these two extremes differ by only 16%, so that even if one took the most conservative possible view of not changing the scale, the qualitative results would still not be changed significantly.

III. INSTANTON CONTENT OF THE GLUON VACUUM

In this section we present the results of cooling the gauge field configurations. Since we are using the quenched approximation, the gluon configurations are not influenced by the quarks and may therefore be fully described independently of the subsequent discussion of hadronic observables.

To provide a clear picture of how cooling extracts the instanton content of a thermalized gluonic configuration, we display in Fig. 1 the action density $S(1,1,z,t)$ and topological charge density $Q(1,1,z,t)$ for a typical slice of a gluon configuration before cooling and after 25 and 50 cooling steps. As one can see, there is no recognizable structure before cooling. Large, short wavelength fluctuations of the order of the lattice spacing dominate both the action and topological charge density. After 25

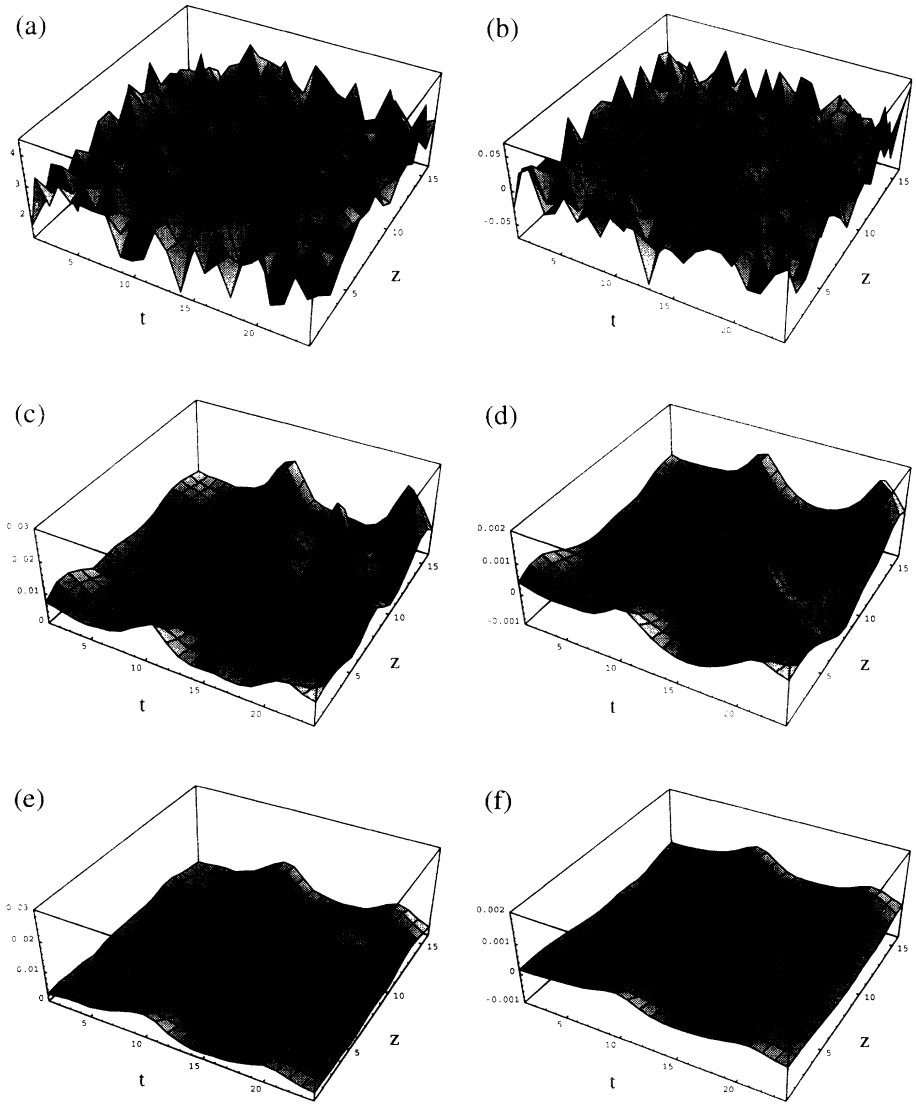

FIG. 1. Cooling history for a typical slice of a gluon configuration at fixed x and y as a function of z and t. The left column shows the action density $S(1,1,z,t)/\beta$ before cooling (a), after cooling for 25 steps (c), and after 50 steps (e). The right column shows the topological charge density $Q(1,1,z,t)$ before cooling (b), after cooling for 25 steps (d), and after 50 steps (f).

cooling steps, three instantons and two anti-instantons can be identified clearly. The action density peaks are completely correlated in position and shape with the topological charge density peaks for instantons and with the topological charge density valleys for anti-instantons. Note that both the action and topological charge densities are reduced by more than two orders of magnitude, so that the fluctuations removed by cooling are several orders of magnitude larger than the topological excitations that are retained. [Also note that because we plot S/β and include the factor $(32\pi^2)^{-1}$ in the definition of Q in Eq. (2.3), the scales in Fig. 1 differ by $4\pi^2/3$.] Since instantons with sizes equal to or smaller than the lattice spacing are strongly distorted on the lattice, they cannot be distinguished from any other short wavelength fluctuations and therefore are presumably cooled away at this point. From Figs. 1(e,f) we see that further cooling to 50 steps results in the annihilation of the nearby instanton–anti-instanton pair but retains the well separated instantons and anti-instanton.

With this orientation from a single configuration, we now consider the ensemble averages of observables as a function of the number of cooling steps shown in Fig. 2. As expected, the action is dominated by the short range modes and is therefore very strongly affected by cooling, decreasing by two orders of magnitude in the first five steps. The topological charge is less sensitive to short range modes, which implies a much milder dependence on cooling. (Note, as discussed below, that our definition of the topological charge is only accurate after several cooling steps have smoothed the configurations.) At cooling step 25, the averaged total action in units of a single instanton action is ~ 65 whereas $\langle Q^2 \rangle$ is

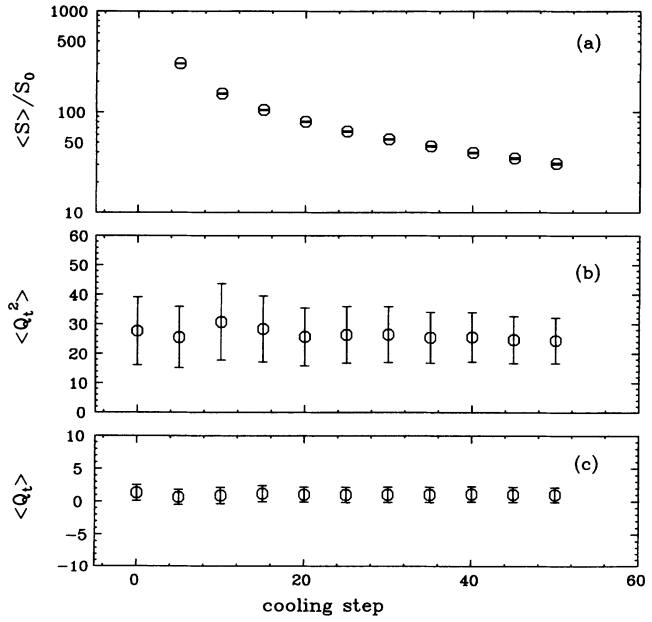

FIG. 2. Mean values of three observables as a function of number of cooling steps. (a) Total action in units of a single instanton action $S_0 = 8\pi^2/g^2$. The uncooled value $\langle S \rangle / S_0 = 20,211$ is far off scale and is not plotted. (b) Topological charge squared. (c) Topological charge.

~ 25. This difference indicates that there are sufficient nearby instanton–anti-instanton pairs in each configuration that we have not yet reached the dilute regime where $\langle Q^2 \rangle \sim A + I$. Since the nearby pairs continue to annihilate under further cooling, we only expect a clear plateau for the topological charge but not for the action in this region of cooling steps. It is only when the configurations are composed of well isolated instantons that plateaus for both action and topological charge would start to emerge. In our case, we expect this will happen beyond 50 cooling steps, where $\langle S \rangle / S_0$ and $\langle Q^2 \rangle$ are nearly equal.

It should be emphasized that, because we used the naive definition for the topological charge density operator, which suffers both additive and multiplicative renormalizations, we cannot use $\langle Q^2 \rangle$ to estimate the topological charge susceptibility when the configurations are not yet smooth. So the first few points in Fig. 2 should not be taken too literally. On the other hand, although the cooled configurations are indeed quite smooth and hence do not suffer from the contamination due to short wavelength fluctuations, the small instanton contribution is also suppressed, giving rise to potential systematic error. One may expect that this suppression should have less effect for calculations with smaller lattice spacing, since the running coupling constant in the instanton action will eventually dynamically suppress small instantons.

The combined information from Figs. 1 and 2 suggests the following qualitative description of our cooled configurations. The configurations cooled with 25 steps are comprised of smooth, clearly recognizable instantons and anti-instantons and still retain many nearby pairs. The configurations cooled with 50 steps consist of more dilute instantons with their total action starting to be dominated by the well isolated peaks. We regard the configurations cooled with 25 steps as providing a more complete description of the instanton content of the original configurations, and will therefore emphasize them in our subsequent calculation of hadronic properties.

In order to characterize the cooled configurations quantitatively and to compare with relevant instanton models, we seek to determine the average instanton size and the instanton–anti-instanton density. To estimate the size we measure the topological charge density correlation function

$$f(x) = \sum_y Q(y)Q(x+y)\,, \tag{3.1}$$

where $Q(y)$ is the topological charge density at point y and the sum is over the whole lattice. The ensemble averages of $f(x)$ at cooling step 25 and 50 are displayed in Fig. 3. The strong peak at small x is the correlation of a single instanton or anti-instanton with itself. The vanishing of $\langle f(x) \rangle$ at large x implies that the topological charge is uncorrelated at this larger distance and thus averages to zero.

If we assume that all instantons are well separated, we would expect that each individual peak can be approximated by the analytic instanton topological charge density

$$Q_\rho(x) = \frac{6}{\pi^2 \rho^4} \left(\frac{\rho^2}{x^2 + \rho^2} \right)^4 , \tag{3.2}$$

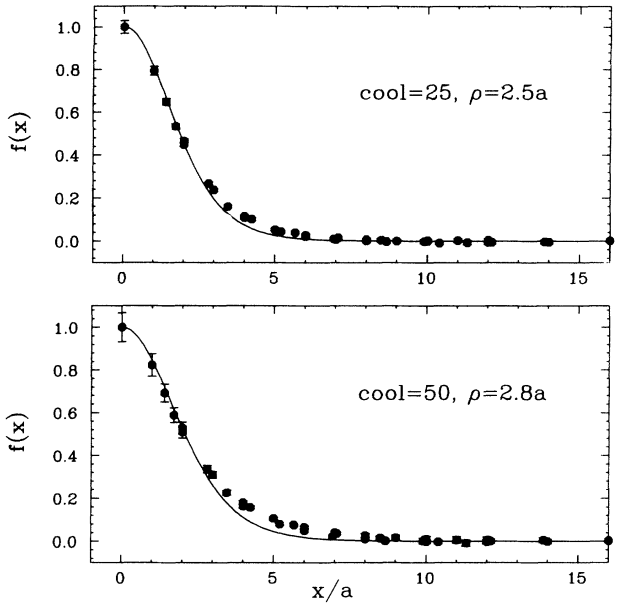

FIG. 3. Topological charge density-density correlation functions after 25 and 50 cooling steps. Lattice measurements are denoted by solid points with error bars. The curves show the best fit obtained using a convolution of the topological charge density for a single instanton size ρ as described in the text. The size parameters ρ are in lattice units.

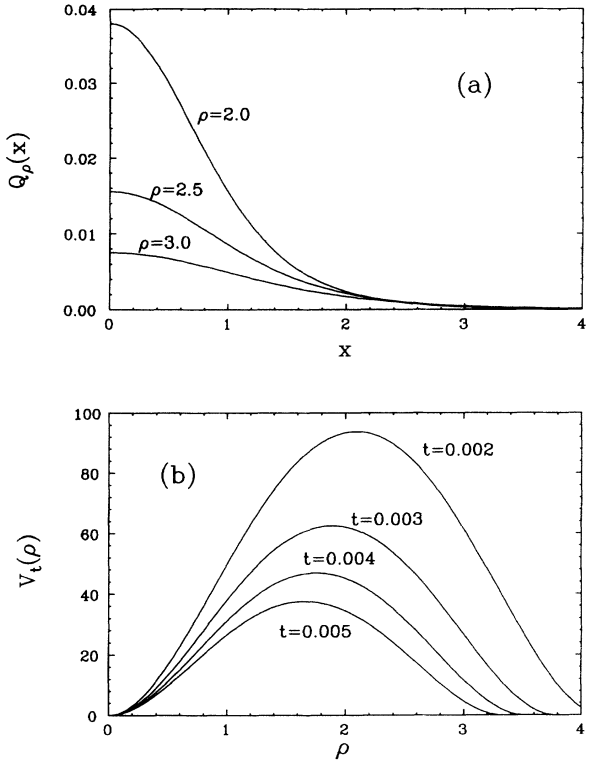

FIG. 4. Plots showing relevant instanton geometry. (a) Topological charge density of a single instanton for the range of sizes ρ dominating the lattice measurements. (b) Cluster size $V_t(\rho)$ [Eq. (3.3)] for the single instanton as a function of its size ρ at several values of threshold t.

where ρ is the size parameter. To show how $Q_\rho(x)$ depends on ρ we plot $Q_\rho(x)$ in Fig. 4(a) for several values of ρ relevant to our present results.

Although in principle one should fit with a distribution of values of ρ, a first approximation is obtained by using a single value of ρ which we will interpret as an average value. A convolution of $Q_\rho(x)$ with itself defines a function which can be used to fit the lattice data with ρ as the fitting parameter. The continuous curves in Fig. 3 are the fitted results with $\rho = 2.5a$ for 25 cooling steps and $\rho = 2.8a$ for 50 cooling steps. The fits fail to reproduce the detailed shape for $x/a \sim 5$. Assuming a uniform distribution for ρ improved the fit somewhat, but we are reluctant to use this method to infer the distribution. We believe that this apparent imperfection of the fitting is due primarily to the nonlinear overlap of instantons as observed in Fig. 1.

One way to estimate the instanton density n, defined as the number of instantons plus the number of anti-instantons per unit volume, is to simply divide the total action by a single instanton action and then divide by the space-time volume, which yields $\langle n \rangle = 64/V$ for 25 cooling steps and $\langle n \rangle = 31/V$ for 50 cooling steps. In addition, once instantons in the cooled configurations were sufficiently dilute to obey Poisson statistics we could also estimate the density using $\langle Q^2 \rangle$, and we note that the two estimates $\langle Q^2 \rangle$ and $\langle S \rangle / S_0$ begin to agree after 50 cooling steps.

As a further consistency check, we have also analyzed the cooled configurations directly by defining clusters. Two adjacent lattice points belong to the same cluster if the product of their topological charge density is greater than the square of a threshold value t. A threshold parameter is necessary since instantons have tails that decay only algebraically. Once again, if instantons are dilute, the size of the cluster for a given ρ and t is approximated by the single continuum instanton formula

$$V_t(\rho) \equiv \int d^4x\, \theta[Q_\rho(x) - t] = \frac{\pi}{2}\rho^2 \left[\left(\frac{6}{\pi^2 t} \right)^{1/4} - \rho \right]^2 . \tag{3.3}$$

We display $V_t(\rho)$ for several values of t in Fig. 4(b). Note that $V_t(\rho)$ has a maximum for each threshold, and observe in Fig. 4(a) how for $t = 0.002$ the maximum is approached as ρ decreases from 3 to 2.5 to 2. In Fig. 5 the distribution of V_t measured in 19 configurations is histogrammed for two thresholds $t = 0.003$ and $t = 0.005$. One distinct feature in Fig. 5 is the sharp sudden drop (indicated by arrows) in each case beyond a maximum value $V_t^{\max}$, reflecting the maxima in $V_t(\rho)$. Since $V_t^{\max}$ depends on the threshold t, we can use Eq. (3.3) to estimate its magnitude and t dependence. The ratios of these maxima at t_1 and t_2 follow the prediction of Eq. (3.3) but the magnitude $V_t^{\max}$ is roughly a factor of 1.5 larger in absolute value than Eq. (3.3). We again attribute this discrepancy to the overlapping between adjacent instantons.

Equation (3.3) may be inverted to express ρ as a function of V_t:

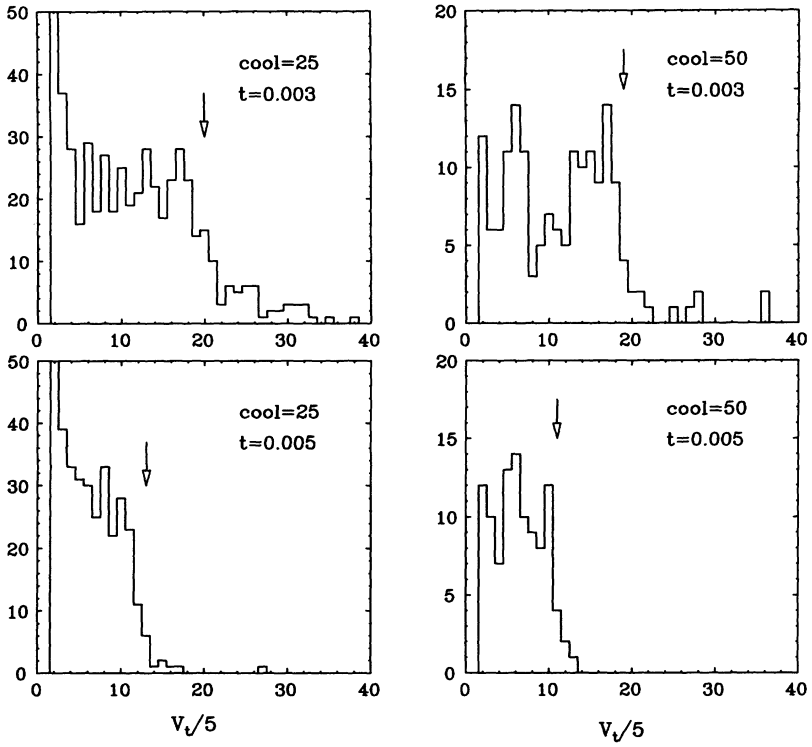

FIG. 5. Distribution of instantons as a function of cluster size. The histograms show the observed counts for given V_t with a bin size 5 using 19 configurations. The number of cooling steps and value of the threshold t are shown in each plot. The arrows indicate the sudden drop at the value $V_t^{\max}$ in each case, as discussed in the text.

$$\rho = \frac{1}{2}\left[\left(\frac{6}{\pi^2 t}\right)^{1/4} \pm \sqrt{\left(\frac{6}{\pi^2 t}\right)^{1/2} - 4\left(\frac{2V_t}{\pi^2}\right)^{1/2}}\right]. \quad (3.4)$$

Since the cooled configurations have very few instantons with $\rho < 2$ lattice units, we may choose the plus sign in Eq. (3.4) and calculate ρ uniquely from V_t. If we correct the overlapping problem in our lattice data by simply dividing the lattice V_t by 1.5, then we can convert Fig. 5 into a histogram in terms of the sizes of instantons. Figure 6 shows the result, including the Jacobian factor $dV_t/d\rho$. These ρ histograms can be regarded as a rough estimate of the instanton size distribution in the cooled configurations. At $t = 0.005$, where the overlapping is

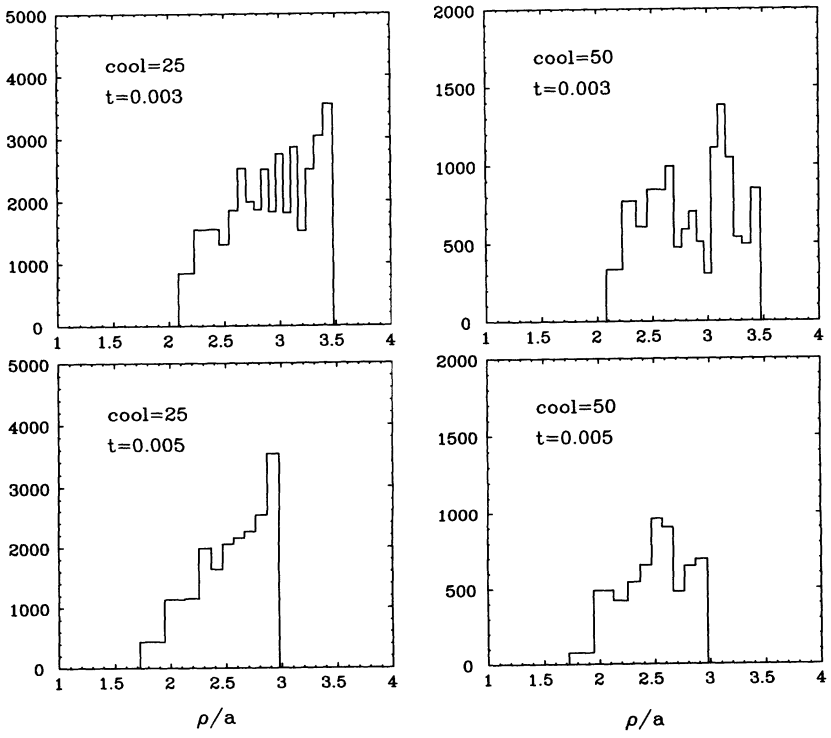

FIG. 6. Distribution of instantons as a function of ρ. Each bin in the histogram of Fig. 5 is converted from V_t to ρ using Eq. (3.4) and multiplied by the Jacobian $dV_t/d\rho$.

TABLE I. Summary of properties of cooled configurations.

Cooling steps	$\langle S\rangle/S_0$	σa^2	a (fm)	ρ (fm)	n (fm^{-4})	χ (MeV^4)
0	20,211	0.18	0.168			
25	64	0.05	0.142	0.36	1.64	$(177)^4$
50	31	0.03	0.124	0.35	1.33	$(200)^4$
Instanton model				0.33	1.0	$(180)^4$

less severe, we see that the distributions are centered around the mean values determined from the topological charge density correlation function, with widths of the order of a half lattice spacing. Note that the factor 1.5 introduced to extract an approximate distribution of ρ does not affect our determination of the average ρ and the density n.

Table I summarizes our result in physical units. The lattice constant a is determined using the proton mass which is measured as described in the next section. The string tension in lattice units was estimated in Ref. [13] using Wilson loops up to sizes 7×4, which corresponds to a distance of around 1 fm. For comparison, the relevant parameters used in instanton models by Shuryak and collaborators [8] are also included.

Finally, we should note that a similar analysis of cooled configurations has previously been carried out in the case of SU(2) with smaller lattices and slightly different techniques [16]. In that work, the positions and magnitudes of peaks in $S(x,y,z,t)$ were used to determine the distribution of sizes of instantons.

IV. HADRONIC OBSERVABLES IN THE COOLED VACUUM

In this section, we present the results for quark propagation and hadron properties in the cooled vacuum and compare them with the corresponding results before cooling.

As in Ref. [2], we extrapolate the masses and vacuum correlation functions calculated at several values of κ to the physical pion mass. The masses extracted from the asymptotic decay of the correlation functions (which agree within errors with the less accurately determined resonance masses obtained from fitting the spectral functions) are tabulated in Table II as a function of κ for 25 and 50 cooling steps. The quality of the chiral extrapolation for masses calculated at 25 cooling sweeps is shown in Fig. 7. We note that M_π^2, M_ρ, M_N, and M_Δ are quite linear over the relevant region of κ. They thus provide a good determination of the values of a and κ_π at which simultaneously $M_\pi = 140$ MeV and $M_N = 940$ MeV. The chiral extrapolation at 50 steps is comparable, and together these extrapolations yield the values for a in Table I and the masses shown in Table III. The chiral extrapolation of the spatial dependence of the ratio of correlation functions $\frac{R(x)}{R_0(x)}$ was carried out using polynomial extrapolation as in Ref. [2]. The quality of the extrapolation was comparable to that shown in Fig. 5 of Ref. [2], and is not presented here to save space.

At this point it is appropriate to address error estimates for the parameters tabulated in Tables II and III. The errors quoted in Table II for hadron masses are standard jackknife errors. As observed in Fig. 1, the magnitude of short range fluctuations in the uncooled gluon configurations is several orders of magnitude larger than the smooth cooled gluon fields, which are reflected in significantly larger statistical errors for uncooled than for cooled configurations. Hence, we were unable to use the asymptotic decay of correlation functions to mea-

TABLE II. Hadron masses in lattice units as a function of κ for 25 and 50 cooling steps. The extrapolated values of κ_c are 0.1285(5) for 25 steps and 0.1283(5) for 50 steps.

25 cooling steps				
κ	$M_\pi a$	$M_\rho a$	$M_N a$	$M_\Delta a$
0.122	0.630(13)	0.713(13)	1.089(21)	1.102(17)
0.124	0.513(16)	0.631(16)	0.958(23)	0.987(19)
0.1255	0.416(20)	0.572(17)	0.862(29)	0.911(22)
0.127	0.301(28)	0.507(16)	0.750(44)	0.839(33)

50 cooling steps				
κ	$M_\pi a$	$M_\rho a$	$M_N a$	$M_\Delta a$
0.122	0.571(12)	0.662(16)	0.999(17)	1.005(29)
0.124	0.454(13)	0.581(15)	0.874(22)	0.896(26)
0.127	0.268(39)	0.471(28)	0.603(63)	0.715(50)

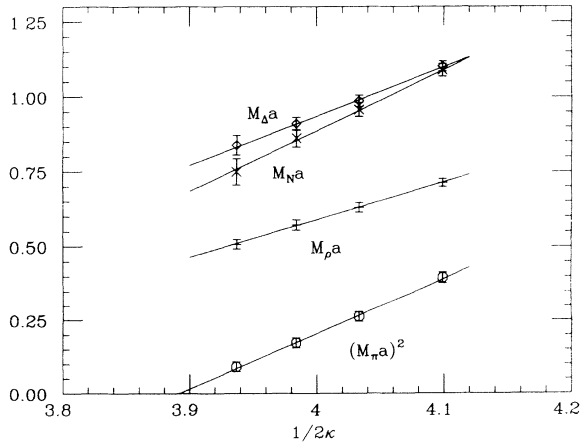

FIG. 7. Chiral extrapolation of hadron masses for configurations with 25 cooling steps. Masses in lattice units calculated at four values of κ are denoted by error bars. The linear extrapolations of M_π^2 to determine $\kappa_c = 0.1285$ and of M_ρ, M_N, and M_Δ to the point at which $M_\pi = 140$ MeV are shown by the straight lines.

TABLE III. Hadron parameters determined from point-to-point vacuum correlation functions for uncooled and cooled configurations.

Channel	Source	M (GeV)	λ	$\sqrt{s_0}$ (GeV)
Vector	Lattice (cool=00)	0.72 ± 0.06	$(0.41 \pm 0.02$ GeV$)^2$	1.62 ± 0.23
	Lattice (cool=25)	0.65 ± 0.03	$(0.385 \pm 0.004$ GeV$)^2$	1.38 ± 0.05
	Lattice (cool=50)	0.70 ± 0.05	$(0.410 \pm 0.005$ GeV$)^2$	1.42 ± 0.04
	Instanton[a]	0.95 ± 0.10	$(0.39 \pm 0.02$ GeV$)^2$	1.50 ± 0.10
	Phenomenology[b]	0.78	$(0.409 \pm 0.005$ GeV$)^2$	1.59 ± 0.02
Pseudoscalar	Lattice (cool=00)	0.156 ± 0.01	$(0.44 \pm 0.01$ GeV$)^2$	< 1.0
	Lattice (cool=25)	0.140[d]	$(0.341 \pm 0.010$ GeV$)^2$	1.05 ± 0.15
	Lattice (cool=50)	0.140[d]	$(0.475 \pm 0.015$ GeV$)^2$	1.80 ± 0.18
	Instanton[a]	0.142 ± 0.014	$(0.51 \pm 0.02$ GeV$)^2$	1.36 ± 0.10
	Phenomenology[b]	0.138	$(0.480$ GeV$)^2$	1.30 ± 0.10
Nucleon	Lattice (cool=00)	0.95 ± 0.05	$(0.293 \pm 0.015$ GeV$)^3$	< 1.4
	Lattice (cool=25)	0.938[e]	$(0.281 \pm 0.004$ GeV$)^3$	1.47 ± 0.13
	Lattice (cool=50)	0.938[e]	$(0.297 \pm 0.004$ GeV$)^3$	1.54 ± 0.11
	instanton[a]	0.960 ± 0.030	$(0.317 \pm 0.004$ GeV$)^3$	1.92 ± 0.05
	Sum rule[c]	1.02 ± 0.12	$(0.324 \pm 0.016$ GeV$)^3$	1.5
	Phenomenology[b]	0.939	——	1.44 ± 0.04
Δ	Lattice (cool=00)	1.43 ± 0.08	$(0.326 \pm 0.020$ GeV$)^3$	3.21 ± 0.34
	Lattice (cool=25)	1.06 ± 0.04	$(0.285 \pm 0.002$ GeV$)^3$	1.91 ± 0.08
	Lattice (cool=50)	1.05 ± 0.09	$(0.298 \pm 0.003$ GeV$)^3$	2.22 ± 0.06
	Instanton[a]	1.440 ± 0.070	$(0.321 \pm 0.016$ GeV$)^3$	1.96 ± 0.10
	Sum rule[c]	1.37 ± 0.12	$(0.337 \pm 0.014$ GeV$)^3$	2.1
	Phenomenology[b]	1.232	——	1.96 ± 0.10

[a]Instanton liquid model of Shuryak *et al.* [8].
[b]Phenomenology estimated by Shuryak and from the particle data book.
[c]QCD sum rule by Belyaev and Ioffe [17].
[d]Used to fix the quark mass.
[e]Used to fix the lattice constant.

sure hadron masses for the uncooled configurations to the same accuracy as the cooled configurations, and so in Table III the uncooled hadron masses are determined from the dispersion relation fit.

One source of systematic errors, as discussed in Ref. [2], is our limited knowledge of the functional form of the spectral function. Thus the resonance plus background parametrization of the spectral function could lead to systematic errors larger than the small statistical errors quoted in Table III. Furthermore, since we fix the hadron mass to its asymptotic value in the dispersion relation fit for the cooled two-point functions, the errors for the fitted parameters are usually underestimated, due to the nonlinear nature of the dispersion relation fitting.

Because of these statistical and systematic errors, we emphasize that the error bars in Table III are underestimates, and care should be taken to avoid misinterpreting the results. For example, one might superficially conclude from the numbers given in Table III that the mass splitting between the Δ and the nucleon is decreased by cooling. However, from Fig. 9 of Ref. [2], we know that the dispersion relation fitted Δ mass is about 20% higher than its asymptotic mass determined by the APE group. Therefore, in order to determine the amount of the mass splitting between the Δ and the nucleon which originates from perturbative one-gluon exchange, one needs to go beyond the numerical precision of the present exploratory calculation.

A. Vacuum correlation functions of hadron currents

The principal results for vacuum correlation functions are presented in Figs. 8 and 9. As in Ref. [2], the individual contribution of the resonance and continuum components of the spectral function, as well as the sum, are plotted. In the top panels of Fig. 8, we show the ratio of interacting to noninteracting current correlation functions, $\frac{R(x)}{R_0(x)}$, in the pseudoscalar channel for uncooled QCD, for 25 cooling steps and for 50 cooling steps. This channel is by far the most attractive of all the meson channels, as reflected in the fact that the correlation function for interacting quarks is roughly 50 times larger than for free quarks, and is thus the only channel to be plotted on a logarthmic scale. Since the pion mass is used to determine the bare quark mass, masses of the pion resonance term in Fig. 8 are constrained to be fixed at 140 MeV. Note that after 25 cooling steps the correlation function is qualitatively similar to the uncooled result, although the magnitude at 1.5 fm is roughly half as large. After an additional 25 cooling steps, the peak grows in strength. Apparently, although the distribution of instantons after 50 steps is more dilute and less representative of the QCD vacuum than after 25 steps, it reproduces the uncooled correlation function slightly better. To assure that this behavior is not a statistical artifact, in this and every other channel we analyzed two independent sets of nine and ten configurations sep-

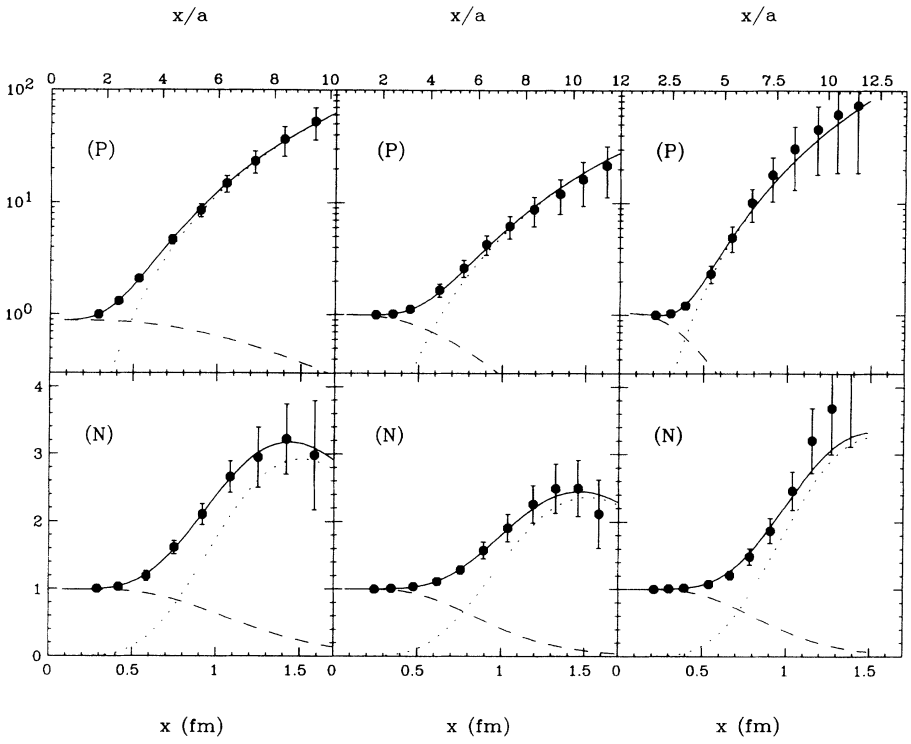

FIG. 8. Comparison of uncooled and cooled vacuum correlation function ratios $\frac{R(x)}{R_0(x)}$ for pseudoscalar currents (P) and nucleon currents (N). The left, center, and right panels show results for uncooled QCD, 25 cooling steps, and 50 cooling steps respectively. The solid points with error bars denote lattice correlation functions extrapolated to $M_\pi = 140$ MeV. The solid lines denote fits to the correlation functions using a three-parameter spectral function, and the dashed and dotted curves show the contributions of the continuum and resonance components of the spectral functions respectively. The upper scale shows the spatial separation in lattice units and the lower scale shows the separation in physical units using the values of a in Table I determined from the nucleon mass.

arately and verified that the same behavior occurred in both cases.

Analogous results for $\frac{R(x)}{R_0(x)}$ in the nucleon channel are shown in the bottom panels of Fig. 8, where again the nucleon mass is constrained to be constant because it is used to determine the lattice spacing. The behavior is similar to that in the pseudoscalar channel. After 25 sweeps, the correlation function is qualitatively similar to the uncooled result. In detail, the peak also appears lower after cooling, although this time it agrees within errors. After an additional 25 sweeps the peak height increases again, agreeing even more closely with the uncooled result.

The ratios of correlation functions $\frac{R(x)}{R_0(x)}$ for the vector channel are shown in the upper panels of Fig. 9. In this case, the ρ mass governing the resonance peak is un-

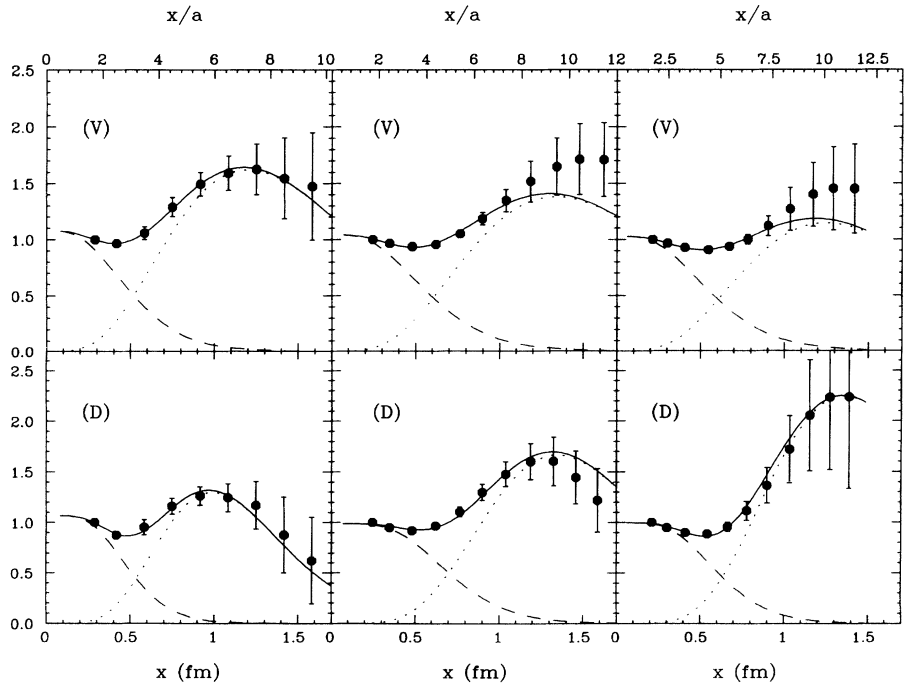

FIG. 9. Comparison of uncooled and cooled vacuum correlation function ratios $\frac{R(x)}{R_0(x)}$ for vector currents (V) and Δ currents (D). The notation is the same as in Fig. 8.

constrained, but as seen in the figure and in Table III, it does not change significantly with cooling. Furthermore, in this channel there is virtually no change in the correlation function ratio with cooling.

Finally, the ratios of correlation functions in the Δ channel are shown in the lower panel. Again, although the position of the Δ peak is unconstrained, it does not shift significantly with cooling. Although the peak height may grow somewhat with cooling, it is also consistent within errors with remaining constant.

The resonance masses M, couplings λ, and continuum thresholds S_0, characterizing these correlation functions in each channel, are tabulated in Table III. These numbers reflect the same features discussed above, and emphasize the similarity of the results after 25 and 50 cooling steps to the uncooled results. In addition, one observes quite general agreement both with phenomenological results where available and with the random instanton model and sum rules.

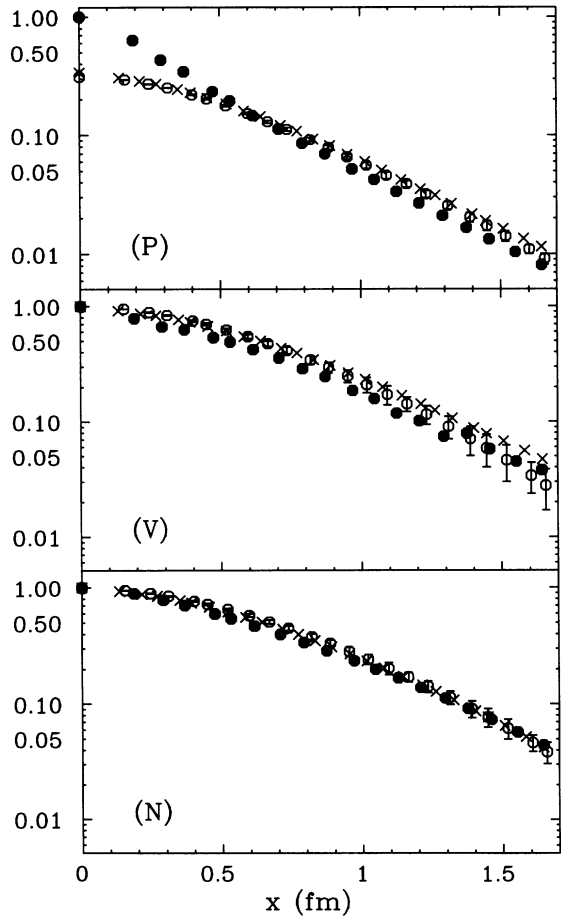

FIG. 10. Comparison of uncooled and cooled density-density correlation functions for the pion, ρ, and nucleon. The solid circles denote the correlation functions calculated with uncooled QCD, the open circles with error bars show the results for 25 cooling steps, and the crosses denote the results for 50 cooling steps. The ρ and pion results are compared for $M_\pi^2 = 0.16$ GeV^2 and the nucleon results are compared for $M_\pi^2 = .36$ GeV^2. As in Figs. 8 and 9, the separation is shown in physical units using values of a from Table I. All correlation functions are normalized to 1 at the origin, except for the cooled pion correlation functions, which are normalized to have the same volume integral as the uncooled pion result. Errors for the uncooled results and for 50 steps, which have been suppressed for clarity, are comparable to those shown for 25 steps.

B. Hadron density-density correlation functions

Density-density correlation functions in the ground state of the π, ρ, and nucleon are shown in Fig. 10. The striking result for both the ρ and the nucleon is the fact that the spatial distribution of quarks is essentially unaffected by cooling—instantons alone govern the gross structure of these hadrons, as indeed they also governed vacuum correlation functions of hadron currents in these same channels.

The only case in which a noticeable change is brought about by cooling is in the short distance behavior of the ground state of the pion. This difference is understandable since in the physical pion, in addition to instanton-induced interactions, there is also a strong attractive hyperfine interaction arising from perturbative QCD which, combined with the $1/r$ interaction, gives rise to the central peak in the uncooled density. In contrast, in the ρ the hyperfine interaction has much less effect, both because it is repulsive and because it is three times weaker. Despite this difference at the origin, which receives small phase space weighting, when the correlation functions are normalized to the same volume integral as in Fig. 10, one observes that the overall size and long distance behavior do not change appreciably with cooling.

It is noteworthy that the cooled density-density correlation functions shown in Fig. 10 for the π, ρ, and nucleon are comparable, within error bars. This uniformity strongly suggests that instantons set the overall spatial scale for these hadrons.

V. SUMMARY AND DISCUSSION

In this work, we have used cooling as an effective filter to remove most of the excitations of the gluon field except for instantons. For example, after 25 cooling steps, when the presence of instantons and anti-instantons is clearly visible in the action density and topological charge density, reduction of the action to 0.3% of its original value has essentially removed all the perturbative, Coulomb-like contributions and reduction of the string tension to 27% of its original value has removed most of the effects of confinement. We have shown that the instanton content of the QCD vacuum extracted by cooling with no free parameters is remarkably similar to that of phenomenological models for which the average instanton size $\rho \sim \frac{1}{3}$ fm and density of the order of 1 fm^{-4} are chosen to reproduce phenomenological values of vacuum quark and gluon condensates.

We have also demonstrated nearly quantitative agreement between cooled and uncooled vacuum hadron current correlation functions in all channels. Similarly we

have shown that the distributions of quarks in the ground state of the ρ and nucleon, as measured by density-density correlation functions, are virtually unchanged. The most noticeable qualitative effect of cooling is the removal of the peak in the pion density-density correlation at short distances arising from the attractive hyperfine interaction, but even for the pion, the gross size and long range behavior are not substantially altered.

The conclusion we draw from these results is that instantons do indeed play a dominant role in light quark propagation in the vacuum and in the low energy structure of hadrons. The picture which emerges is that a light quark propagating in the QCD vacuum does not really respond to the details of the huge, short wavelength fluctuations seen in the top of Fig. 1, but rather hops between the localized quark states corresponding to the zero modes associated with the instantons which become visible in the lower panels of Fig. 1.

Although we believe these results provide substantial evidence for the role of instantons, we recognize several significant limitations. Despite our best efforts to monitor the effects of cooling, cooling remains an imprecise filter. In addition to exploring alternative filters and characterizing the effect of cooling more completely it would also be worthwhile to complement this work with a companion calculation in which one modified the Monte Carlo algorithm to emphasize other excitations and suppress instantons.

There are several significant problems associated with use of the quenched approximation. Clearly, when nearly zero modes are playing an important role in quark propagation, it is also important to include the small weight arising from the small eigenvalue in the determinant. In addition, in studying the instanton content of the vacuum, it is important to include fermion feedback so that, for example, the tendency of quark-antiquark pairs to bind instanton–anti-instanton pairs is included. Hence, in view of the significant role of instantons in the quenched results reported in this work, it is important to explore the effect of dynamical fermions.

ACKNOWLEDGMENTS

It is a pleasure to thank Edward Shuryak for extensive discussions concerning this work. In addition, we acknowledge useful discussions with Ken Johnson, Michail Polikarpov, and Janos Polonyi. We also thank the National Energy Supercomputer Center for supercomputer resources. This work was supported in part by funds provided by the U.S. Department of Energy (DOE) under Contracts Nos. DE-AC02-76ER03069 and DE-FG06-88ER40427, and the National Science Foundation under Grant No. PHY 90-13248.

[1] E. V. Shuryak, Rev. Mod. Phys. **65**, 1 (1993).
[2] M.-C. Chu, J. M. Grandy, S. Huang, and J. W. Negele, Phys. Rev. Lett. **70**, 225 (1993); Phys. Rev. D **48**, 3340 (1993).
[3] K. Barad, M. Ogilvie, and C. Rebbi, Phys. Lett. **143B**, 222 (1984); Ann. Phys. (N.Y.) **168**, 284 (1986).
[4] M.-C. Chu, M. Lissia, and J. W. Negele, Nucl. Phys. **B360**, 31 (1991).
[5] M. Lissia, M.-C. Chu, J. W. Negele, and J. M. Grandy, Nucl. Phys. **A555**, 272 (1993).
[6] K. Teo and J. W. Negele, in *Lattice '93*, Proceedings of the International Symposium, Dallas, Texas, 1993, edited by T. Draper, S. Gottlieb, A. Soni, and D. Toussaint [Nucl. Phys. B (Proc. Suppl.) (in press)].
[7] E. V. Shuryak, Nucl. Phys. **B203**, 93 (1982); **B203**, 116 (1982); **B203**, 140 (1982); **B302**, 559 (1988); **B302**, 599 (1988); **B319**, 521 (1989); **B319**, 541 (1989); **B328**, 85 (1989); **B328**, 102 (1989); in *Lattice '93* [6].
[8] E. V. Shuryak and J. J. M. Verbaarschot, Nucl. Phys. **B410**, 55 (1993); T. Schäfer, E. V. Shuryak, and J. J. M. Verbaarschot, Nucl. Phys. **B412**, 143 (1994).
[9] D. I. Dyakanov and V. Yu Petrov, Nucl. Phys. **B245**, 259 (1984); **B272**, 457 (1986).
[10] B. Berg, Phys. Lett. **104B**, 475 (1981).
[11] M. Teper, in *Lattice '90*, Proceedings of the International Symposium, Tallahassee, Florida, 1990, edited by U. M. Heller, A. D. Kennedy, and S. Sanielevici [Nucl. Phys. **B** (Proc. Suppl.) **20**, 159 (1991)].
[12] N. Cabibbo and E. Marinari, Phys. Lett. **119B**, 387 (1982).
[13] M.-C. Chu and S. Huang, Phys. Rev. D **45**, 2446 (1992).
[14] M.-C. Chu, J. M. Grandy, M. Lissia, and J. W. Negele, in *Lattice '91*, Proceedings of the International Symposium, Tsukuba, Japan, 1991, edited by M. Fukugita *et al.* [Nucl. Phys. **B** (Proc. Suppl.) **26**, 412 (1992)].
[15] M. Campostrini, A. Di Giacoma, H. Panagopoulos, and E. Vicari, Nucl. Phys. **329**, 683 (1990).
[16] M. I. Polikarpov and A. I. Veselov, Nucl. Phys. **B297**, 34 (1988).
[17] B. L. Ioffe, Nucl. Phys. **B188**, 317 (1981); V. M. Belyaev and B. L. Ioffe, Zh. Eksp. Teor. Fiz. **83**, 976 (1982) [Sov. Phys. JETP **56**, 547 (1982)].

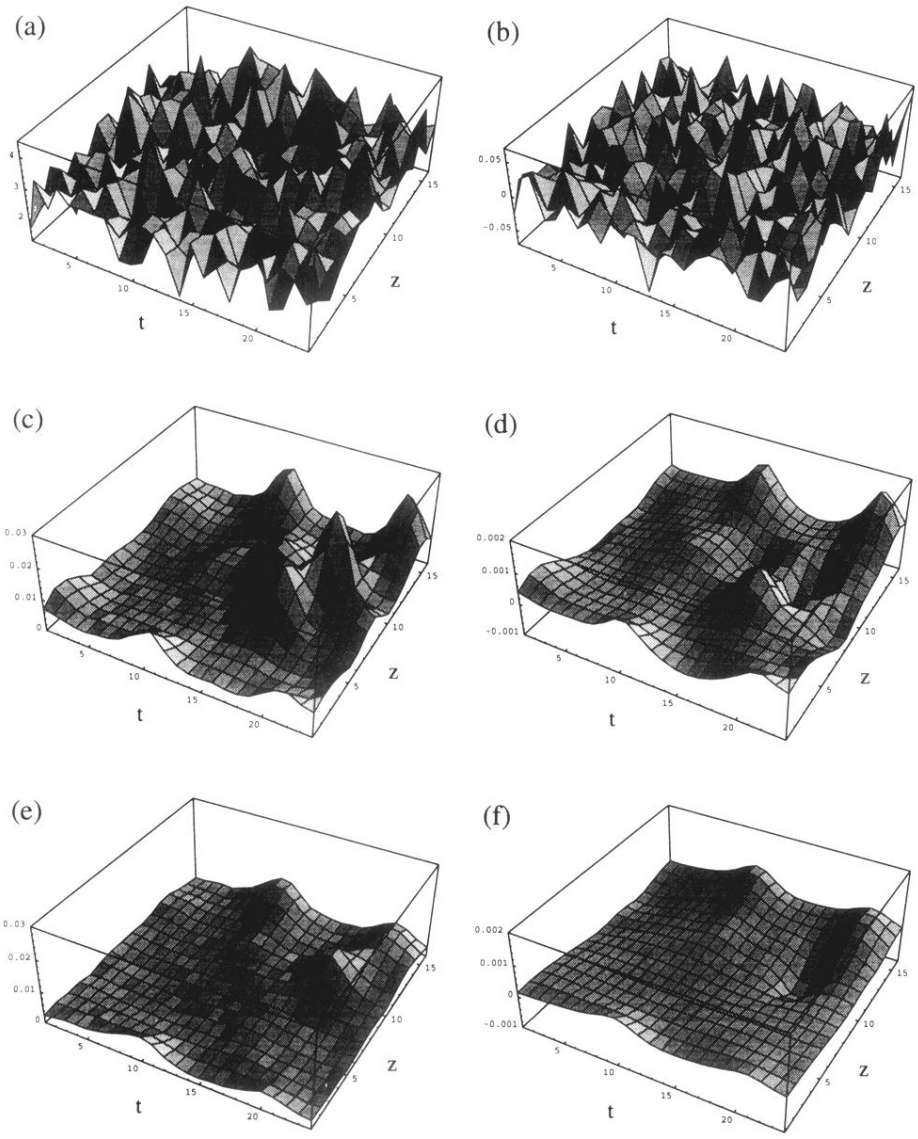

FIG. 1. Cooling history for a typical slice of a gluon configuration at fixed x and y as a function of z and t. The left column shows the action density $S(1,1,z,t)/\beta$ before cooling (a), after cooling for 25 steps (c), and after 50 steps (e). The right column shows the topological charge density $Q(1,1,z,t)$ before cooling (b), after cooling for 25 steps (d), and after 50 steps (f).